Supporting Information for "Mars Dust Storm Effects in the Ionosphere and Magnetosphere and Implications for Atmospheric Carbon Loss"

Xiaohua Fang [1], Yingjuan Ma [2], Yuni Lee [3], Stephen Bougher [4], Guiping Liu [5], Mehdi Benna [3], Paul Mahaffy [3], Luca Montabone [6,7], David Pawlowski [8], Chuanfei Dong [9], Yaxue Dong [1], and Bruce Jakosky [1]

[1]Laboratory for Atmospheric and Space Physics, University of Colorado, Boulder, Colorado, USA

[2]Department of Earth, Planetary and Space Sciences, University of California, Los Angeles, California, USA

[3]NASA Goddard Space Flight Center, Greenbelt, Maryland, USA

[4]Department of Climate and Space Sciences and Engineering, University of Michigan, Ann Arbor, Michigan, USA

[5]Space Sciences Laboratory, University of California, Berkeley, California, USA

[6]Space Science Institute, Boulder, Colorado, USA

[7]Laboratoire de Météorologie Dynamique/IPSL, Sorbonne Université, Paris, France

[8]Physics and Astronomy Department, Eastern Michigan University, Ypsilanti, Michigan, USA

[9]Department of Astrophysical Sciences and Princeton Plasma Physics Laboratory, Princeton University, Princeton, New Jersey, USA

Contents of this file

Figures S1 to S4

Additional Supporting Information (Files uploaded separately)

This supplement provides additional information regarding the impact of the Mars 2017 late-winter regional dust storm (dust event 1) in the ionosphere and magnetosphere.

References

Vignes, D., et al. (2000), The solar wind interaction with Mars: Locations and shapes of the bow shock and the magnetic pile-up boundary from the observations of the MAG/ER Experiment onboard Mars Global Surveyor, *Geophys. Res. Lett., 27(1)*, 49-52, doi:10.1029/1999GL010703.

Corresponding author: Xiaohua Fang, Xiaohua.Fang@lasp.colorado.edu

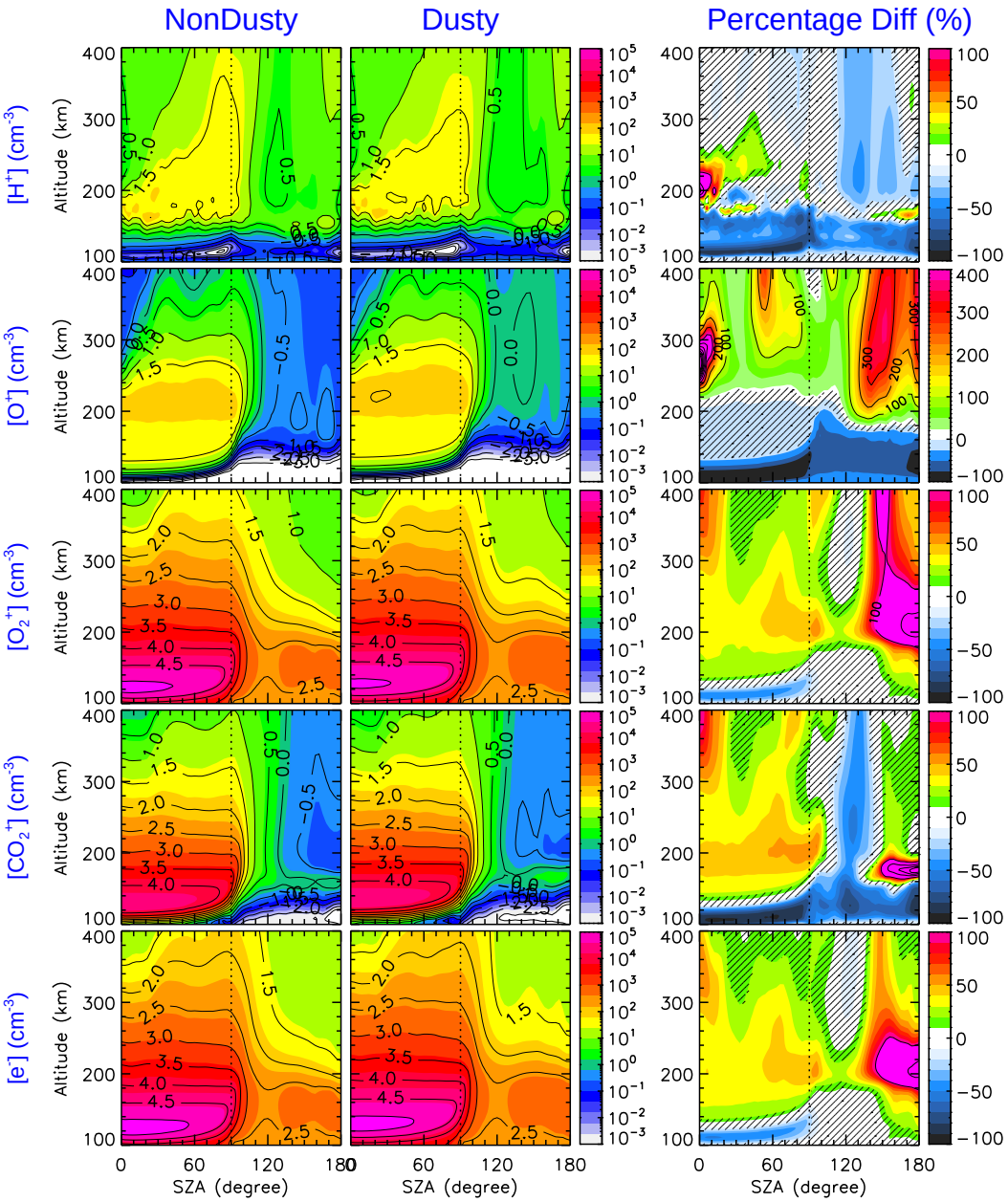

Figure 1. MHD-calculated ionospheric density disturbances for dust event 1 as a function of SZA and altitude. The left two columns present the SZA-averaged ionospheric densities under nondusty and dusty atmospheric conditions, respectively. The right column shows their percentage differences, i.e., dusty values minus nondusty divided by nondusty. From top to bottom, the panels show the results for different ionospheric species, using different color scales for the percentage changes. In the right column, the contour lines indicate a percentage change of every 100% interval, particularly useful on the nightside where the relative difference may be sufficiently high to make the color scale saturated. The hatched areas mark the places having a modest change, where the absolute percentage difference is less than 20%.

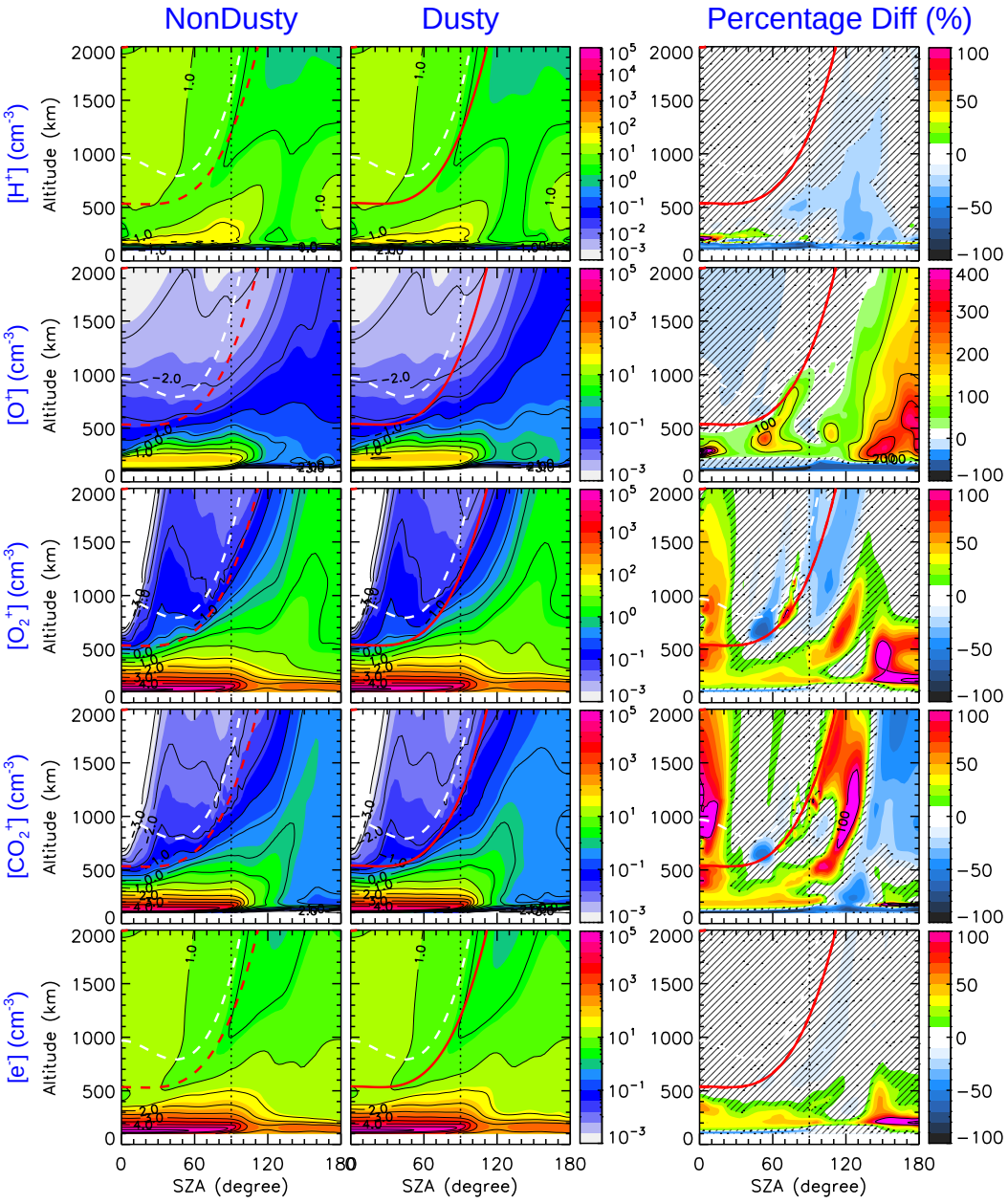

Figure 2. Similar to Figure 1 but including the results of the induced magnetosphere during dust event 1, with the altitude limit extended up to as high as 2000 km. The average location of the induced magnetospheric boundary, which is obtained using a conic section fit, is shown as red dashed (solid) lines for nondusty (dusty) conditions. The empirical location by *Vignes et al.* [2000] is superposed as white dashed lines for reference. Note that our MHD-derived bow shock is also shown but partly at the upper left corners of the panels, which is located mostly higher than 2000 km altitude except near subsolar in this specific case.

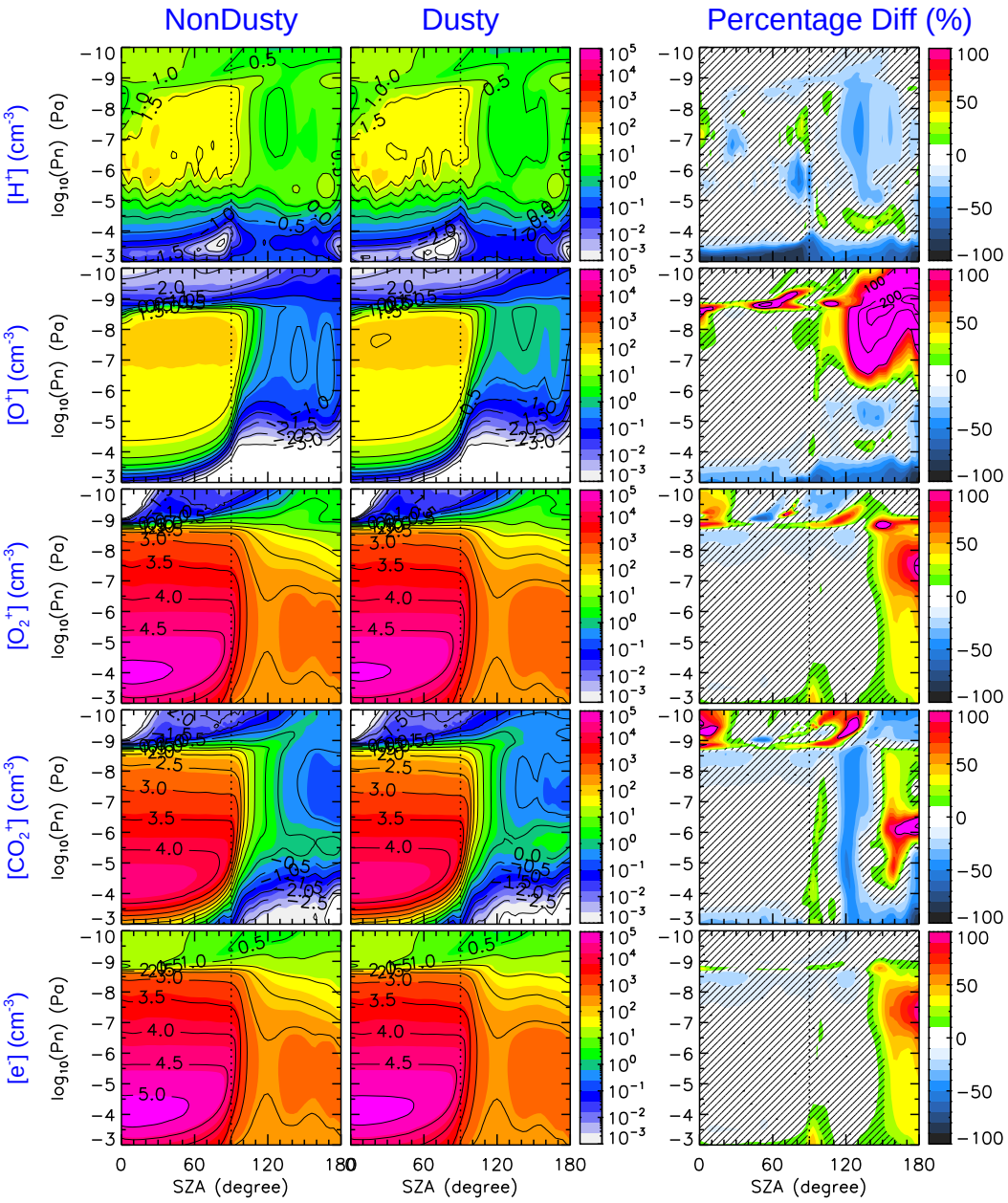

Figure 3. Similar to Figures 1 and 2 except that the results for dust event 1 are presented at atmospheric pressure levels. The pressure axis has been reversed in correspondence with altitude increase from the bottom to the top.

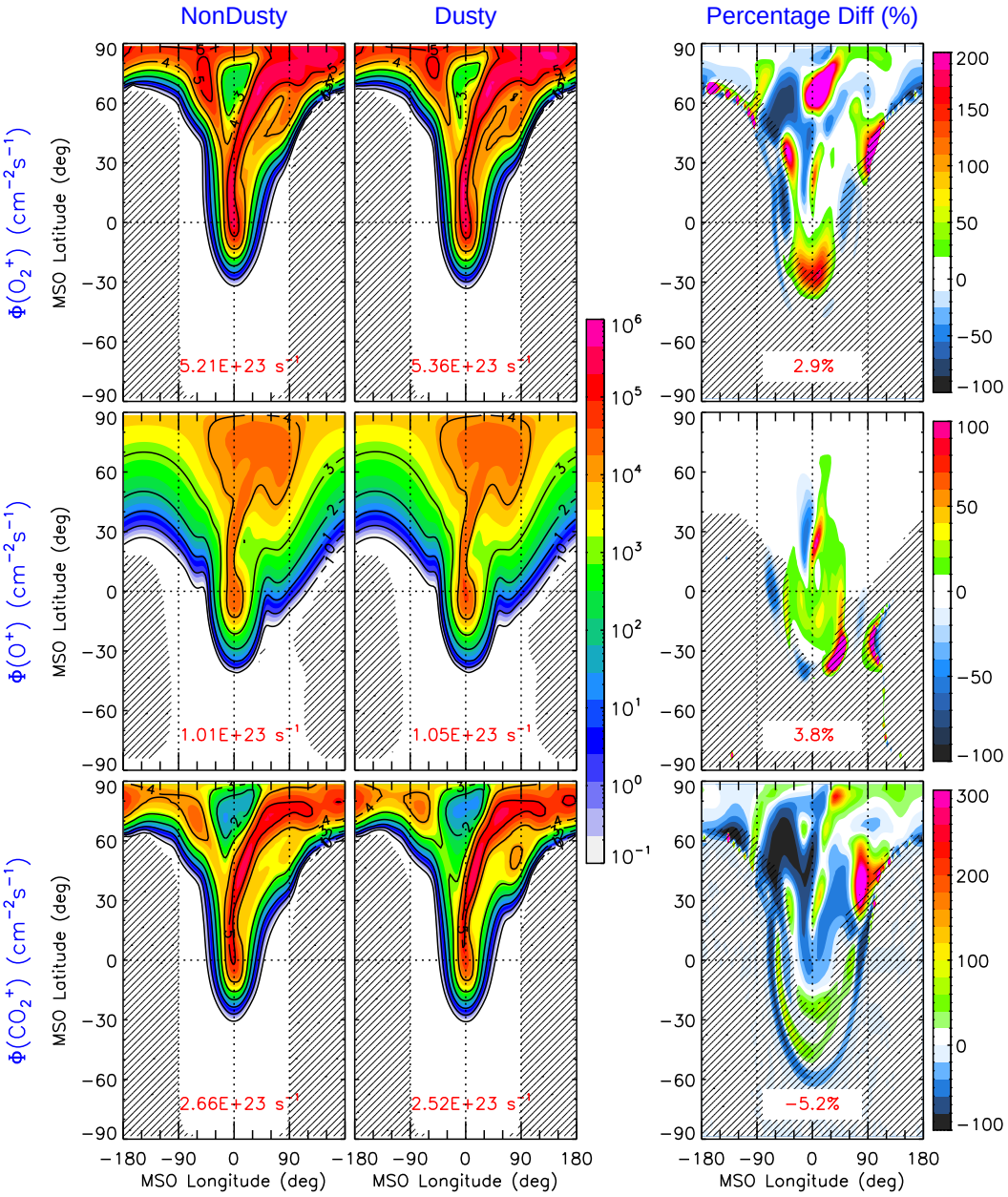

Figure 4. Comparison of the MHD-calculated planetary ion fluxes escaping through the spherical surface at a radial distance of 6 R_M from the Mars center during dust event 1. The panels from top to bottom show the results for O_2^+, O^+, and CO_2^+, respectively. The left two columns present the results under nondusty and dusty atmospheric conditions, respectively, as a function of MSO longitude and latitude. The MSO latitude is measured from the MSO equatorial plane, on which 0° longitude and ±180° longitude point toward the antisunward and sunward directions, respectively. The hatched areas mark negative fluxes, that is, for ion velocities having a radially inward component. The spherically integrated loss rates are indicated on the bottom of the panels. In the right column, we show the percentage difference between the left two columns. The hatched areas correspond to insignificant ion fluxes of less than 10 $cm^{-2}s^{-1}$, where the relative comparison is less meaningful. The percentage differences of the total loss rates are indicated on the panels.